# PHOCUS: Physics-Based Deconvolution for Ultrasound Image Enhancement

Felix Duelmer[1,2,3], Walter Simson[4], Mohammad Farid Azampour[1,2], Magdalena Wysocki[1,2], Angelos Karlas[1,5], and Nassir Navab[1,2]

[1]Technical University of Munich, Munich, Germany
[2]Munich Center for Machine Learning (MCML), Munich, Germany
[3]Helmholtz Centre Munich, Neuherberg, Germany
[4]Stanford University, Stanford, USA
[5]German Centre for Cardiovascular Research, Munich, Germany

MICCAI 2024 Marrakesh MOROCCO

Paper Code

## Motivation

- Ultrasound Resolution is limited by e.g. diffraction and finite apertures that **constrain diagnostic capabilities**
- Retrieving the **exact location** of reflectors and scatterers based on a processed B-mode image **is difficult** due to unknown acquisition parameters and processing step

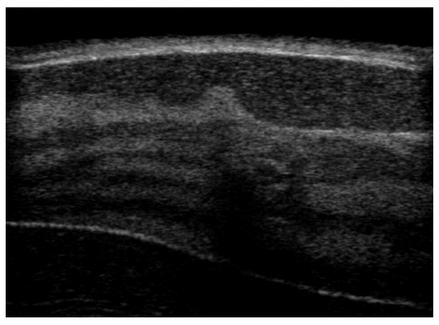

## Image Formation Process

### Signal Processing Pipeline

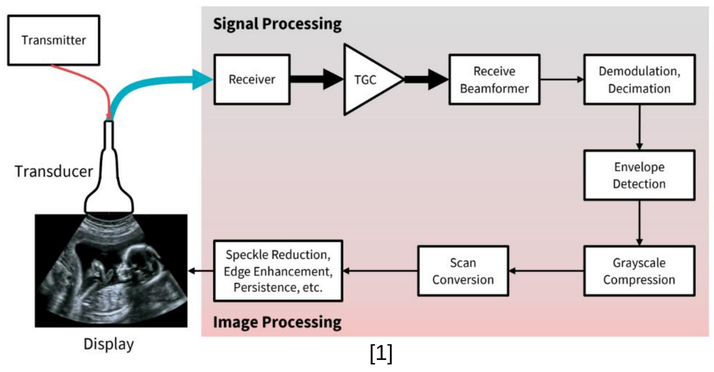


[1]

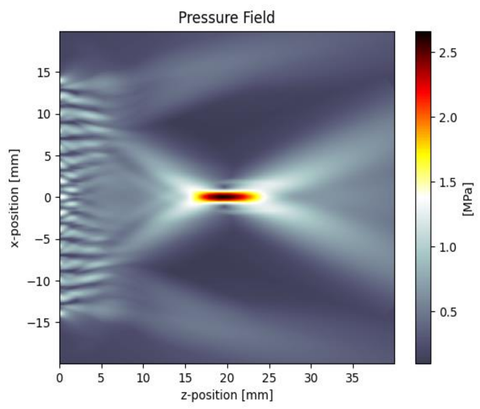


### Convolutional Model

The interaction between acoustic wave and tissue can be modeled by a convolution between a filter and the echogenicity map.

The filter is called the **Point Spread Function** (PSF) of the imaging system and incorporates acquisition parameters such as aperture size, acquisition frequency, etc.

$$y(z') = h(z') \otimes \gamma(z') + n(z')$$

$y$ : radio-frequency data, $h$ : PSF, $\gamma$ = echogenicity map, $n$ : gaussian noise, $*$ : convolution

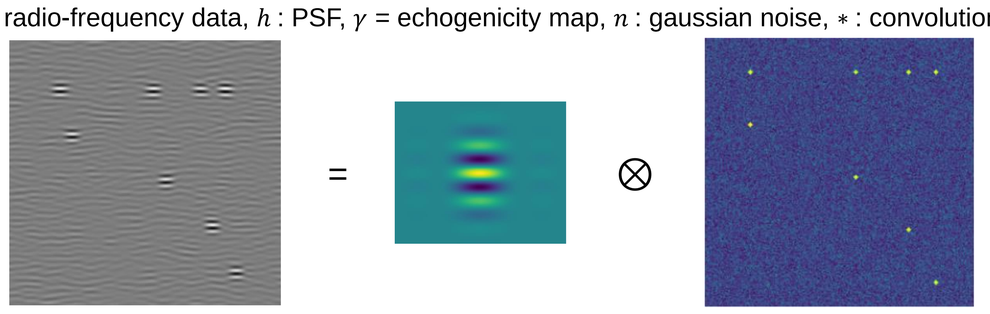

## Deconvolution

Deconvolution model **estimate the PSF** of the imaging system to **convolve** the acquired image with **its inverse**.

**Blind vs. Non-Blind Deconvolution**

Blind Deconvolution: Estimate the PSF **based on the acquired data** [2]

Non-Blind Deconvolution: Estimate an **analytical** form of the PSF **based on equations** [3]

The derived PSF is used as the filter in deconvolution algorithms, such as the Wiener Filter or the Richardson-Lucy Algorithm.

→ But these methods **lack flexibility**, necessitate **careful tuning of regularizers**, and require **high computational resources** when applied to large datasets

## Point-Spread-Function

Adapting the model from [4] we define the PSF to:

$$h(x', z') = h_{lat}(x') \otimes h_{ax}(z')$$

The **lateral pressure** distribution at the focal point can be written as a **convolution** of the Fourier transformation of the **transmit** $A_T$ and **receive** function $A_T$ :

$$h_{lat}(x' \mid \lambda, D, r) = \mathcal{F}(A_T) \otimes \mathcal{F}(A_T)$$
$$= D^2 \mathrm{sinc}^2\left(\frac{Dx'}{r\lambda}\right)$$

We remove the envelope detection step, in accordance with [3], and model the **axial signal** to:

$$h_{ax}(z' \mid \sigma_z) = exp\left(-\frac{z'^2}{2 * \sigma_z^2}\right)$$

Where $\sigma_z$ = scaling factor based on the number of cycles for the axial pulse.

Where $D$ = Aperture and $\lambda$ = wavelength.

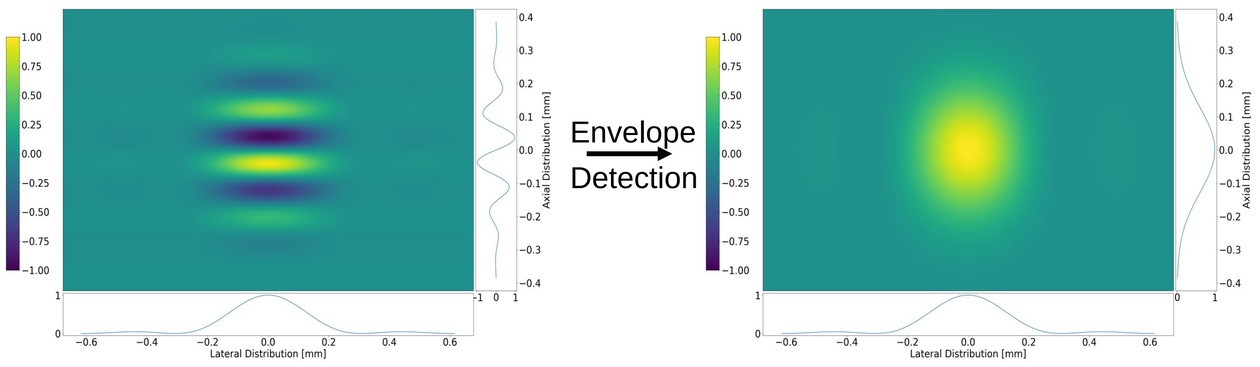


## Proposed Approach

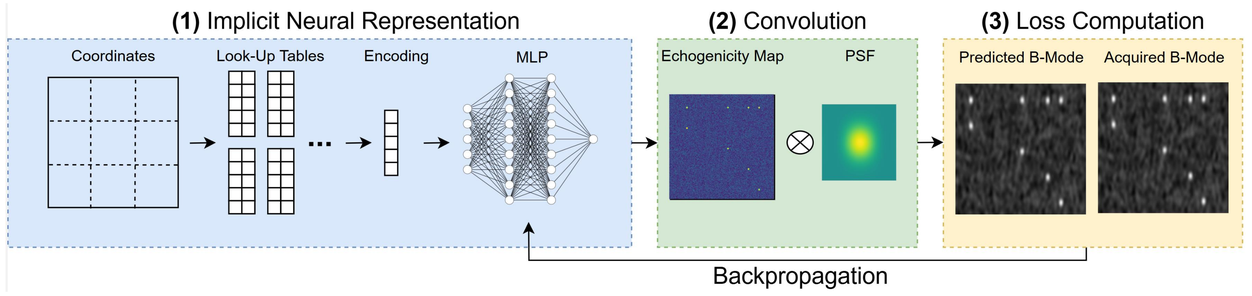


### (1) Implicit Neural Representation (INR)

- For a given **input coordinate x**, the surrounding grid vertices lead to an entry in the **learnable** look-up tables. The look-up tables contains one vector per vertice, which is used as the input to a linear interpolation.
- An L-dimensional **multi-resolution grid** provides L entries which are concatenated to form the input to the MLP. The MLP outputs a single scalar **echogenicity value**.

### (2) Differentiable Image processing pipeline

- The output of the MLP **is convolved** with an isotropic PSF
- A **differentiable** signal **processing pipeline** transforms the convolved data via log-compression to the imaging domain

### (3) Loss Computation

- Loss function= Combination of a total variation loss (TV), structural similarity index (SSIM) loss, and a mean-squared error (MSE) loss

## Results

### Synthetic Results (CIRS Phantom)

- Comparison with the Richardson-Lucy Algorithm
- Synthetic images are created with a known PSF (f = 10 MHz, pulses= 5, f-number = 2.0)

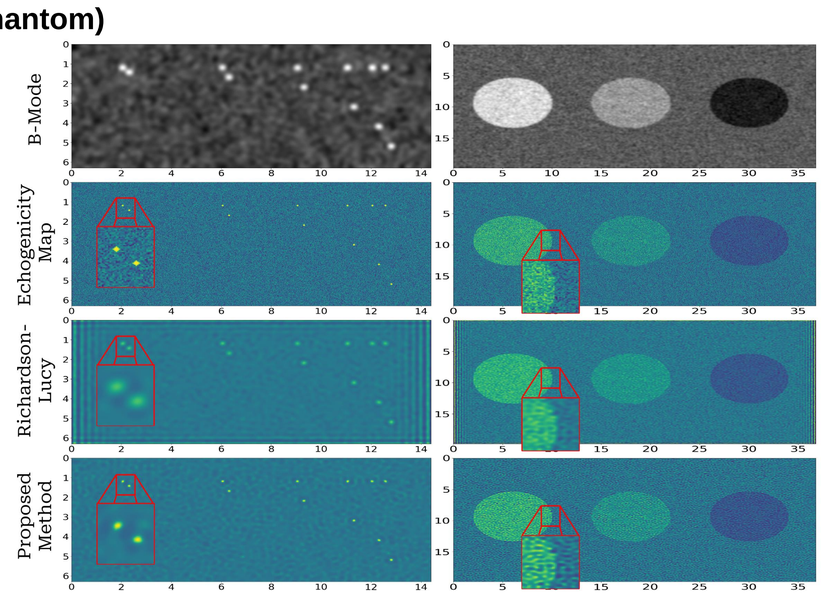


| | Wire Targets | | Cylindrical Inclusions | |
|---|---|---|---|---|
| | PSNR | SSIM | PSNR | SSIM |
| Richardson-Lucy | 17.35 | 0.06 | 16.89 | 0.21 |
| Proposed Method | **17.85** | **0.07** | **17.85** | **0.29** |

### In-Silico Results (CIRS Phantom)

**10 of 12 wires** are correctly identified with a mean radius of 0.053 mm (+- 0.01), expected value is 0.040 mm, based on processed data (thresholding, filtering and clustering)

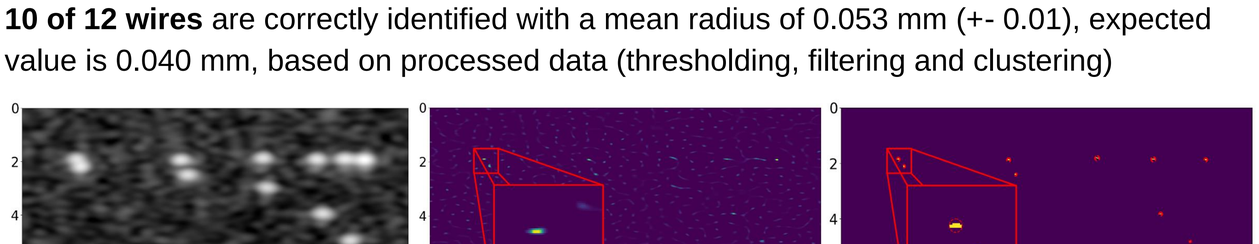

Acquired B-Mode Images | Predicted Echogenicity Map | Processed Echogenicity Map

### In-Vivo Results (Carotid Data)

Using the predicted **echogenicity map** we can change the “acquisition parameters” to generate new B-Mode Images

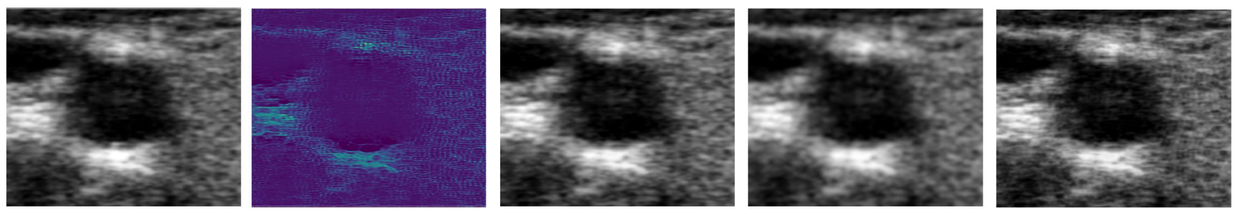

B-Mode Image | Predicted Echogenicity Map | Reconstructed B-Mode | Lower Frequency | Higher Frequency

## Summary

We effectively leverage an **INR** for learning a continuous representation of the **echogenicity map** based only on the B-mode image and a deconvolutional model including a **fully differentiable** rendering pipeline which integrates a PSF that is **based on equations** derived from the wave equations.

## References

[1] Hyun, Dongwoon. “Advanced Ultrasound Imaging”, Summer semester 2023, Stanford, University. Lecture.
[2]: Li, X., Zhang, X., Fan, C., Chen, Y., Zheng, J., Gao, J., & Shen, Y. (2024). Deconvolution based on sparsity and continuity improves the quality of ultrasound image. Computers in Biology and Medicine, 169, 107860.
[3]: Dalitz, C., Pohle-Frohlich, R., & Michalk, T. (2015). Point spread functions and deconvolution of ultrasonic images. IEEE transactions on ultrasonics, ferroelectrics, and frequency control, 62(3), 531-544
[4] Walker, W. F., & Trahey, G. E. (1998). The application of k-space in pulse echo ultrasound. IEEE transactions on ultrasonics, ferroelectrics, and frequency control, 45(3), 541-558.
[5] Müller, T., Evans, A., Schied, C., & Keller, A. (2022). Instant neural graphics primitives with a multiresolution hash encoding. ACM transactions on graphics (TOG), 41(4), 1-15.